nature chemical biology

BRIEF COMMUNICATION

PUBLISHED ONLINE: 13 APRIL 2014 | DOI: 10.1038/NCHEMBIO.1502

Dynamics and hydration explain failed functional transformation in dehalogenase design

Jan Sykora[1,6], Jan Brezovsky[2,6], Tana Koudelakova[2,6], Maryna Lahoda[3,4], Andrea Fortova[2], Tatsiana Chernovets[1], Radka Chaloupkova[2], Veronika Stepankova[2], Zbynek Prokop[2,5], Ivana Kuta Smatanova[3,4], Martin Hof[1]* & Jiri Damborsky[2,5]*

We emphasize the importance of dynamics and hydration for enzymatic catalysis and protein design by transplanting the active site from a haloalkane dehalogenase with high enantioselectivity to nonselective dehalogenase. Protein crystallography confirms that the active site geometry of the redesigned dehalogenase matches that of the target, but its enantioselectivity remains low. Time-dependent fluorescence shifts and computer simulations revealed that dynamics and hydration at the tunnel mouth differ substantially between the redesigned and target dehalogenase.

© 2014 Nature America, Inc. All rights reserved.

Enzymes catalyze conversion of various chemical compounds in a very specific and effective manner, which makes them applicable in chemical industry and pharmaceutics. However, natural catalysts often do not meet the needs of industry and must be improved by protein engineering. The protein engineering approaches aimed at constructing enzymes with improved properties benefit from *in silico* methods[1], including bioinformatic analysis, molecular modeling and *de novo* protein design. *De novo* protein design[2], used in the computational design of active enzymes[3], has yielded active enzymes for reactions not catalyzed by naturally occurring biocatalysts, including the Kemp elimination[4], retro-aldol[5] and bimolecular Diels-Alder reactions[3]. However, proteins generated in this way do not compete with naturally occurring enzymes, which have substantially higher catalytic rates and selectivity, and so directed evolution must be applied to generate practically useful biocatalysts[6–9]. Additional catalytic and recognition elements need to be added to the *de novo* designs to move the constructs closer to the native biocatalysts, as has been recently demonstrated with the Kemp eliminase[10]. Thus, an outstanding question in the field is why enzyme redesign is not more successful. In this work, we explore this question in the context of efforts to transplant the active site and access tunnel from a highly enantioselective enzyme to a nonselective one in a stepwise manner. We chose enantioselectivity as the target property as it depends on both the binding and the catalytic steps and is considered as a hallmark of molecular recognition.

Haloalkane dehalogenases are enzymes of the α-β hydrolase superfamily, which catalyze the cleavage of the carbon-halogen bond in halogenated hydrocarbons by an S_N2 mechanism. Recently, we studied the enantioselectivity of DbjA from *Bradyrhizobium japonicum* USDA11019 (ref. 11) and of DhaA from *Rhodococcus rhodochrous* NCIMB13064 (ref. 12). Both enzymes have an identical catalytic pentad[13] and show enantioselectivity for α-bromoesters; however, only DbjA shows enantioselectivity for β-bromoalkanes[14]. This unique enantioselectivity of DbjA for β-bromoalkanes is modulated by the fragment ^{138}HHTEVAEEQDH^{150} (hereafter termed the ERB fragment, for extra region of *B. japonicum*)[14]. Given the assumption of ideal geometry of the transition states, this enantioselectivity of DbjA for β-bromoalkanes could, in principle, be transferred to DhaA by inserting the ERB fragment and accumulating eight single-point mutations in the active site and access tunnel (**Fig. 1**).

CD spectroscopy analysis revealed that insertion of the ERB fragment into DhaA affects the protein structure, but the correct folding was reconstituted during transplantation of single-point substitutions into its active site and the access tunnel (**Supplementary Results**, **Supplementary Fig. 1**). Improvement of folding corresponded with a gradual increase in structural

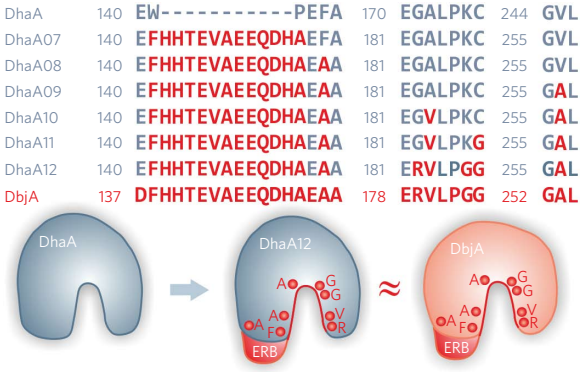

Figure 1 | Transplantation of the active site and the access tunnel from DbjA to DhaA. The amino acid sequences of DbjA and DhaA have 47% sequence identity and 59% sequence similarity; their active site and access tunnel differ by the ERB fragment and eight amino acid substitutions: W141F, P153A, F155A, G182R, A183V, K186G, C187G and V256A (in red). The active site and the access tunnel of DbjA were transplanted to DhaA by the cumulative introduction of mutations through DhaA7–12. DhaA12 has the same active site and access tunnel as DbjA (in red; **Fig. 2d**,**e**), whereas the rest of its protein context is identical to that of the parental DhaA (in gray). There are eight additional mostly conservative substitutions in the second shell and eight in the third shell of the active sites (**Supplementary Table 6**).

[1]J. Heyrovsky Institute of Physical Chemistry of the ASCR, v.v.i., Academy of Sciences of the Czech Republic, Prague, Czech Republic. [2]Loschmidt Laboratories, Department of Experimental Biology and Research Centre for Toxic Compounds in the Environment (RECETOX), Faculty of Science, Masaryk University, Brno, Czech Republic. [3]Faculty of Science, University of South Bohemia in Ceske Budejovice, Ceske Budejovice, Czech Republic. [4]Institute of Nanobiology and Structural Biology ASCR, v.v.i., Nove Hrady, Czech Republic. [5]International Clinical Research Center, St. Anne's University Hospital Brno, Brno, Czech Republic. [6]These authors contributed equally to this work. *e-mail: martin.hof@jh-inst.cas.cz or jiri@chemi.muni.cz

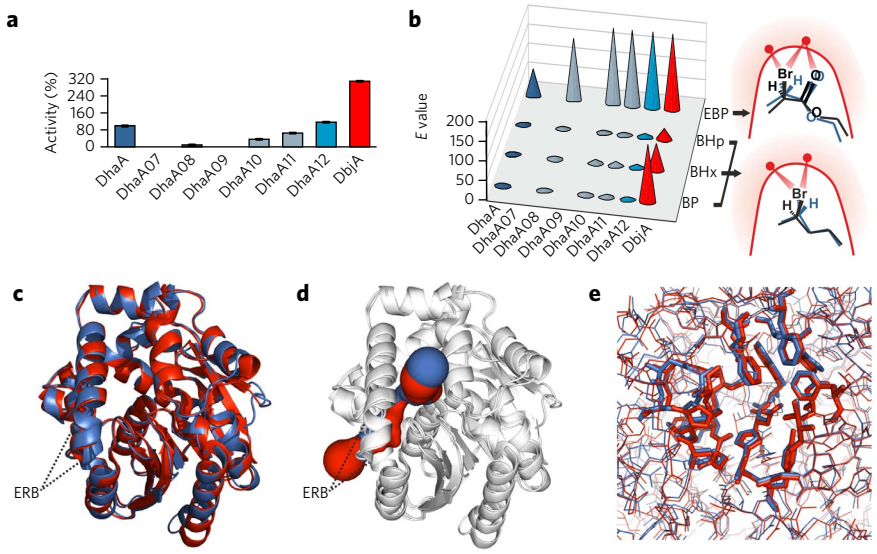

Figure 2 | Structural and biochemical properties of wild types and variants. (**a**) The activity measurements were in good correspondence with CD spectra (**Supplementary Fig. 1**), demonstrating that variants with altered structure exhibited considerably reduced activity for 1,3-dibromopropane. Enzyme activity is shown relative to the specific activity of DhaA (39.6 nmol s^{-1} mg^{-1} of enzyme). Data represent mean values ± s.d. calculated from duplicate experiments. (**b**) Enantioselectivity of the active enzymes quantified by the *E* value was evaluated with racemic mixtures of 2-bromopentane (BP), 2-bromohexane (BHx), 2-bromoheptane (BHp) and ethyl 2-bromopropionate (EBP). The s.e. of the fit for *E* values were in the 5–25% range. (**Supplementary Table 2**). The different effect of the mutations on enantiodiscrimination of β-bromoalkanes versus α-bromoesters comes from the distinct structural basis of enantioselectivity: β-bromoalkane interacts with the active site via two hydrogen bonds, whereas α-bromoester does so via three hydrogen bonds[14]. Preferred (*R*) enantiomers are in black, and nonpreferred (*S*) enantiomers are in blue; hydrogen bonds are represented by red triangles. (**c**) Comparison of the crystal structures of DhaA12 (in blue) and DbjA (in red). The ERB fragment is indicated by dotted lines. (**d**) Overlay of the access tunnels calculated by CAVER[25]. The tunnels are shown in surface representation. (**e**) Superposition of the active site residues is represented in sticks.

stability (**Supplementary Fig. 1** and **Supplementary Table 1**) and activity toward 1,3-dibromopropane (**Fig. 2a**). We measured enantioselectivity with racemic mixtures of ethyl 2-bromopropionate, 2-bromopentane, 2-bromohexane and 2-bromoheptane for all of the active variants (**Fig. 2b** and **Supplementary Table 2**). Whereas enantioselectivity with the α-bromoester was improved already in the intermediate variant DhaA08, we observed only very little effect on the enantioselectivity for β-bromoalkanes, even with all of the introduced mutations.

To investigate how well the structure of the active site and the access tunnel of DhaA12 matches that of DbjA, we determined the crystal structure of DhaA12 to 1.8-Å resolution by protein crystallography (**Supplementary Table 3**) and compared it with that of DbjA, previously determined to the same resolution[14] (**Fig. 2c**,**d**). This comparison revealed atomic-level agreement in the active site and the access tunnel, with all atom r.m.s. deviation values of this functionally important region being 0.7 Å (**Fig. 2e**). The r.m.s. deviation of the transplanted ERB fragment and substituted residues was 1.6 Å and 1.1 Å, respectively (**Supplementary Fig. 2**). This agreement was even more pronounced for the catalytic pentads with r.m.s. deviation <0.3 Å (**Supplementary Fig. 3**). This result confirmed successful transplantation of the active site and the access tunnel of DbjA into DhaA in a geometrical sense. Yet, the enantioselectivity of DhaA12 with β-bromoalkanes did not reach the level of DbjA (**Fig. 2b**), suggesting that other factors, in addition to the geometrical characteristics, influence the enzyme's enantioselectivity.

Previous mutational analysis of DbjA suggests the importance of a flexible ERB fragment near the tunnel mouth for enantioselectivity toward β-bromoalkanes, and a thermodynamic analysis reveals the role of both enthalpic and entropic contributions to enantiodiscrimination[14]. Therefore, we characterized the dynamics and hydration, which have been proposed to affect the enzyme activity[15–17], at the tunnel mouth of DhaA, DhaA12 and DbjA using the time-dependent fluorescence shift (TDFS)[18–21]. The magnitude and relaxation time of the TDFS respectively provide information on the hydration and dynamics[22] of the protein segment in the intimate fluorophore environment[19,23]. Because positioning of the

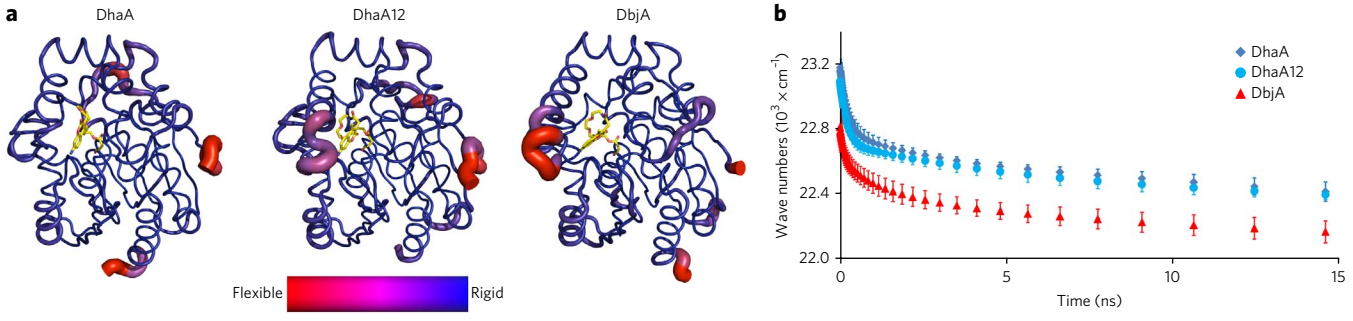

Figure 3 | Dynamics and hydration of wild type and variants. (**a**) The dynamics of the residues quantified by backbone B factors from molecular dynamics simulations and represented by the color scale mapped onto average structures of simulated proteins and by the thickness of their ribbon. The average structures of covalently bound fluorescent probes are shown in yellow sticks. (**b**) TDFS expressed as the time dependence of the maxima of time-resolved emission spectra for the variants DhaA, DhaA12 and DbjA. The TDFS, containing information on both dynamics and hydration, does not differ notably for DhaA and DhaA12, but it does, however, substantially vary for DbjA. Four experiments were performed for DhaA and DbjA, and duplicate measurements were carried out in the case of DhaA12. Data represent mean values ± s.d. A detailed comparison of those TDFS values is given in **Supplementary Table 4**.

© 2014 Nature America, Inc. All rights reserved.

chromophore within the protein scaffold is the main prerequisite for interpretability of the TDFS, we confirmed the single location of the coumarin probe by MALDI-TOF (**Supplementary Fig. 4**), fluorescence quenching (**Supplementary Fig. 5**) and crystallographic analysis (data not shown). It is worth noting that the long arm linker of the used fluorophore may lead to a ground state microheterogeneity, which might influence the interpretation of TDFS. We cannot fully exclude this effect. However, the emission spectra recorded at various acrylamide concentrations do not show pronounced differences in their positions, indicating rather homogeneous positioning of the chromophore.

Analysis of the TDFS together with molecular dynamics simulations revealed that the tunnel mouth of DbjA was the most flexible and hydrated of the three enzymes (**Supplementary Tables 4** and **5**). The geometrical metamorphosis of DhaA to DbjA, achieved by inserting the ERB fragment and introducing eight point mutations, did not result in dynamics and hydration comparable to that of DbjA. Although the flexible regions were correctly positioned within the protein structures, the amplitudes of motions remained very different (**Fig. 3a**). The integral relaxation time, inversely related to the dynamics of the tunnel mouth, was lowest for DbjA (2.8 ns), whereas it was notably larger for both DhaA and DhaA12 (4.1 ns and 3.8 ns, respectively). The hydration and polarity of the dye microenvironment followed the order DbjA > DhaA12 > DhaA (**Supplementary Table 5**). The dye was considerably more solvated in DbjA than in the DhaA12-DhaA pair. The presence of the ERB fragment in DbjA had a large effect on TDFS results (**Fig. 3b**), indicating its role in the dynamics and polarity at the tunnel mouth, which in turn correlated with high enantioselectivity of DbjA toward β-bromoalkanes. This high enantioselectivity of more flexible and hydrated recognition sites is counterintuitive but is supported by the data from thermodynamics analysis, highlighting the importance of entropic contribution toward enantioselectivity[14]. The ERB fragment inserted into DhaA12 did not have such dynamics and hydration, presumably because of the different protein context, and this enzyme lacked enantioselectivity toward β-bromoalkanes.

It has been proposed that protein design can fail for three main reasons: (i) the proposed model is incorrect, (ii) the designed active site geometry is not realized within the protein scaffold or (iii) the overall protein context might not be compatible with the catalytic reaction[24]. In this study, we took DbjA as a fully functional model of the active site for enantioselective catalysis of halogenated substrates, and we transplanted this active site into the compatible scaffold of DhaA. Therefore, the first two arguments do not apply in this case. Instead, we have provided experimental evidence that the geometrically optimized enzyme DhaA12 largely differs from the target DbjA in its dynamics and hydration and that those factors are relevant for enzyme enantioselectivity. Our observations suggest that the protein context, consisting of protein geometry, dynamics and hydration, is important for enzymatic catalysis and should be simultaneously considered in computational protein design. One way to integrate these factors into the design strategy is to complement design of static structure by molecular dynamic simulations in explicit solvent. However, deeper understanding of entropic contributions to enzymatic catalysis is needed to computationally identify the protein structures with properly engineered dynamics and hydration components.

Received 4 December 2013; accepted 25 February 2014; published online 13 April 2014

Methods

Methods and any associated references are available in the online version of the paper.

Accession codes. Protein Data Bank (PDB). The refined model of DhaA12 and its corresponding structure factor were deposited under accession code 3SK0.

References

1. Damborsky, J. & Brezovsky, J. *Curr. Opin. Chem. Biol.* **19**, 8–16 (2014).
2. Koehl, P. & Levitt, M. *J. Mol. Biol.* **293**, 1161–1181 (1999).
3. Siegel, J.B. *et al. Science* **329**, 309–313 (2010).
4. Röthlisberger, D. *et al. Nature* **453**, 190–195 (2008).
5. Jiang, L. *et al. Science* **319**, 1387–1391 (2008).
6. Kries, H., Blomberg, R. & Hilvert, D. *Curr. Opin. Chem. Biol.* **17**, 221–228 (2013).
7. Khersonsky, O. *et al. Proc. Natl. Acad. Sci. USA* **109**, 10358–10363 (2012).
8. Khare, S.D. *et al. Nat. Chem. Biol.* **8**, 294–300 (2012).
9. Giger, L. *et al. Nat. Chem. Biol.* **9**, 494–498 (2013).
10. Blomberg, R. *et al. Nature* **503**, 418–421 (2013).
11. Sato, Y. *et al. Appl. Environ. Microbiol.* **71**, 4372–4379 (2005).
12. Kulakova, A.N., Larkin, M.J. & Kulakov, L.A. *Microbiology* **143**, 109–115 (1997).
13. Chovancová, E., Kosinski, J., Bujnicki, J.M. & Damborsky, J. *Proteins* **67**, 305–316 (2007).
14. Prokop, Z. *et al. Angew. Chem. Int. Edn Engl.* **49**, 6111–6115 (2010).
15. Eisenmesser, E.Z. *et al. Nature* **438**, 117–121 (2005).
16. Henzler-Wildman, K. & Kern, D. *Nature* **450**, 964–972 (2007).
17. Bhabha, G. *et al. Science* **332**, 234–238 (2011).
18. Jimenez, R., Fleming, G.R., Kumar, P.V. & Maroncelli, M. *Nature* **369**, 471–473 (1994).
19. Halle, B. & Nilsson, L. *J. Phys. Chem. B* **113**, 8210–8213 (2009).
20. Jesenská, A. *et al. J. Am. Chem. Soc.* **131**, 494–501 (2009).
21. Chang, C.-W. *et al. Proc. Natl. Acad. Sci. USA* **107**, 2914–2919 (2010).
22. Jurkiewicz, P., Cwiklik, L., Jungwirth, P. & Hof, M. *Biochimie* **94**, 26–32 (2012).
23. Nilsson, L. & Halle, B. *Proc. Natl. Acad. Sci. USA* **102**, 13867–13872 (2005).
24. Baker, D. *Protein Sci.* **19**, 1817–1819 (2010).
25. Chovancova, E. *et al. PLoS Comput. Biol.* **8**, e1002708 (2012).

Acknowledgments

We thank D. Baker (University of Washington) for helpful comments on the manuscript. This work was supported by the European Regional Development Fund (CZ.1.05/1.1.00/02.0123), the Czech Ministry of Education (LO1214), the Czech Science Foundation (P208/12/G016 to J.S. and M.H. and P503/12/0572 to J.D.) and the 'Employment of Best Young Scientists for International Cooperation Empowerment' program (CZ1.07/2.3.00/30.0037 to J.B.), financed by both the European Social Fund and the state budget of the Czech Republic. The Academy of Sciences is acknowledged for the Praemium Academie award (M.H.). CERIT Scientific Cloud is acknowledged for providing access to their computing facilities under the Center CERIT Scientific Cloud program (CZ.1.05/3.2.00/08.0144).

Author contributions

J.S. and T.C. conducted fluorescence spectroscopy measurements. J.B. performed molecular modeling. T.K. and A.F. constructed the mutants. T.K. and Z.P. biochemically characterized the mutants. T.K., V.S. and R.C. conducted CD spectroscopy measurements. M.L. and I.K.S. determined the crystal structure. M.H. and J.D. conceived and supervised the project. J.S., J.B., T.K., M.H. and J.D. wrote the paper together.

Competing financial interests

The authors declare no competing financial interests.

Additional information

Supplementary information is available in the online version of the paper. Reprints and permissions information is available online at http://www.nature.com/reprints/index.html. Correspondence and requests for materials should be addressed to M.H. or J.D.

© 2014 Nature America, Inc. All rights reserved.

ONLINE METHODS

Preparation of variants and their biochemical characterization. *DNA manipulations.* Enzymes used for DNA manipulations were obtained from Takara Bio (Kyoto) or New England BioLabs (Ipswich) unless stated otherwise. *Escherichia coli* strains used in this study were DH5α, BL21 and BL21 (DE3). Plasmids carrying the gene for ampicillin resistance, pUC18 (Takara Bio), pAQN and pET21b (Novagen), were used for basic cloning manipulations, mutagenesis or expression of recombinant genes[26]. The constructs pAQN-*dbjA*, pAQN-*dbjA*+His280Phe and pAQN-*dhaA*+His272Phe were prepared, followed by overexpression and purification of the corresponding enzymes, as described previously[11,14,20]. Plasmids with genes of cumulative mutants (pUC18-*dhaA07* to pUC18-*dhaA12*) and genes coding enzyme for fluorescence measurements (pAQN-*dhaA12*+His283Phe) were constructed by inverted PCR with KOD Plus polymerase (Toyobo) or by using a QuikChange (Stratagene) site-directed mutagenesis kit according to manufacturer's instructions. The *dhaA* gene (DDBJ/GenBank/EMBL accession number AF060871) in pUC18 served as an initial template for cumulative mutagenesis. Recombinant genes *dhaA* and *dhaA07–12* were subsequently subcloned into the pET21b expression vector downstream of the T7 promoter and in front of the sequence coding the His_6 tag.

Overexpression and purification. DhaA12(+His283Phe) was overexpressed in *E. coli* BL21 in 2l of LB medium (Sigma-Aldrich) at 37 °C. The *dhaA* gene variants in pET21b were expressed similarly but in the strain *E. coli* BL21 (DE3) and at 18 °C. The induction of enzyme expression at 30 °C was initiated by the addition of IPTG to a final concentration of 0.5 mM. The cells were harvested and disrupted by sonication using a Soniprep 150 (Sanyo Gallenkamp). The supernatant was used after centrifugation at 21,000*g* for 1 h. Enzymes with His_6 C-terminal tags were purified to homogeneity from cell-free extracts using a Ni-nitrilotriacetic acid resin (Qiagen) in the equilibrating buffer (50 mM phosphate buffer, pH 7.5, containing 500 mM sodium chloride and 10 mM imidazole). Unbound and weakly bound proteins were washed out. The tagged enzymes were eluted with buffer containing 500 mM imidazole. The active fractions were pooled and dialyzed overnight against 50 mM phosphate buffer (pH 7.5).

CD spectroscopy. CD spectra (190–260 nm) were recorded at 22 °C using a Jasco J-810 spectropolarimeter (Jasco). Thermal unfolding was measured in triplicate by monitoring the ellipticity at 222 nm over the temperature range 20–80 °C, with a resolution of 0.1 °C and at a heating rate of 1 °C/min. Recorded thermal denaturation curves were fitted to sigmoidal curves using the software Origin 6.1 (OriginLab), and the melting temperature, T_m, was evaluated as a midpoint of the normalized thermal transition. T_m is defined as the temperature at which half of the enzyme is in its unfolded state.

Activity assay. All of the halogenated chemicals used were purchased from Sigma-Aldrich and had purity >95%. Initial velocity measurements were performed in 100 mM glycine buffer (pH 8.6) in 25-ml Reacti Flasks (Supelco) closed with Mininert Valves (Supelco) at 37 °C. The activity assay was conducted in duplicate with 1.5 mM 1,3-dibromopropane. After addition of an enzyme, dehalogenase activity was monitored by determination of substrate concentrations with gas chromatograph or of released halides in periodically withdrawn samples with mercuric thiocyanate and ferric ammonium sulfate[27]. The change in color was measured spectrophotometrically at 460 nm. The substrate concentration was assayed by the Trace GC 2000 gas chromatograph equipped with the flame ionization detector (Thermo Finnigan) and the DB-FFAP capillary column (J&W Scientific).

Enantioselectivity assay. Kinetic resolution experiments were performed at room temperature (21 °C). Racemic mixtures of 2-bromopentane, 2-bromohexane, 2-bromoheptane or ethyl 2-bromopropionate were dissolved in 50 mM Tris-sulfate buffer (pH 8.2) in screw-capped reaction vessels. Enzymatic reaction was initiated by addition of an enzyme and monitored by periodical withdrawal of samples from the reaction mixture. Samples were extracted to diethyl ether containing 1,2-dichloroethane as an internal standard, dewatered by anhydrous Na_2SO_4 and analyzed by the Hewlett-Packard 6890 gas chromatograph (Agilent Technologies) equipped with the flame ionization detector and the Chiraldex B-TA or G-TA chiral capillary column (Sigma-Aldrich). Enantioselectivity was quantified by the *E* value, defined as the ratio of catalytic efficiency of conversion of the preferred (*R*) over the nonpreferred (*S*) enantiomer: E value = $(k_{cat,R}/K_{m,R})/(k_{cat,S}/K_{m,S})$, where k_{cat} is the catalytic constant and K_m is the Michaelis constant. To estimate the *E* values, the equations describing competitive Michaelis-Menten kinetics were fitted by numerical integration to time courses of changes in substrate concentrations obtained from the kinetic resolution experiments using Global Kinetic Explorer program (KinTek). Numerical integration was performed using the Bulirsch-Stoer algorithm with adaptive step size, and nonlinear regression to fit data was based on the Levenberg–Marquardt method. Final fitting was performed by nonlinear regression based on the simulation with the standard error of the fit between 5% and 25%.

Fluorescence spectroscopy. *Labeling of enzymes with coumarin 120 dye.* Proteins in 50 mM phosphate buffer (pH 7.5) were diluted to a final concentration of 50 μM and mixed with 15 μM HaloTag coumarin ligand (Promega). After 15 min incubation at 37 °C, the mixture was loaded on Ni-nitrilotriacetic acid resin (Qiagen) pre-equilibrated with 20 mM potassium phosphate buffer (pH 7.5) containing 0.5 M NaCl and 10 mM imidazole. The unbound ligand was washed out, and the protein-ligand complex bound by the protein's C-terminal His_6 tag to the resin was subsequently eluted with 20 mM potassium phosphate buffer (pH 7.5) with 0.5 M NaCl and 300 mM imidazole. The protein-ligand sample was dialyzed against 20 mM glycine buffer (pH 8.2) to remove imidazole, and NaCl and was immediately used for fluorescence measurements.

Steady-state fluorescence measurements. Steady-state excitation and emission spectra were recorded on Fluorolog-3 spectrofluorometer FL3-11 (Horiba Jobin Yvon) equipped with a Xenon-arc lamp at 10 °C. All of the spectra were collected in 1-nm steps (2-nm bandwidths were chosen for both the excitation and emission monochromators). The temperature in the cuvette holder was maintained within ±0.1 °C using a water-circulating bath. When performing the fluorescence quenching measurements, the samples were excited at 350 nm, and the emission was detected at 450 nm. The aliquots of the acrylamide were added directly to the protein sample in the cuvette with a Hamilton syringe, and the cuvette contents were stirred continuously. The recorded values of the fluorescence intensity were corrected for dilution effects. Three experiments were performed for DhaA and DbjA, and duplicate quenching measurements were carried out in the case of DhaA12.

Time-resolved fluorescence measurements. Fluorescence decays were collected by using IBH 5000 U SPC equipment (Horiba Jobin Yvon) with a picosecond diode laser (IBH NanoLED 11, a peak wavelength of 370 nm, a pulse width of 80 ps and a 1-MHz repetition rate) and a cooled R3809U-50 microchannel plate photomultiplier (Hamamatsu) with 30-ps time resolution. Emission decays were recorded at a series of wavelengths spanning the steady-state emission spectrum (400–490 nm) in 5-nm steps. To eliminate scattered light, a 399 nm cut-off filter was used. The signal was kept below 2% of the light source repetition rate, and data were collected in 4,096 channels (0.028 ns per channel) until the peak value reached 5,000 counts. Fluorescence decays were fitted to multiexponential functions using the iterative reconvolution procedure with IBH DAS6 software (Horiba Jobin Yvon). Time-resolved emission spectra (TRES) were obtained by the spectral reconstruction method as described[18]. To determine the position of the spectra $\nu(t)$ (i.e., their maxima), the TRES were fitted by a log-normal function. The time evolution of the TRES maximum was treated as described previously[20], yielding the parameters concluded in **Supplementary Table 4**. Four experiments were performed for DhaA and DbjA, and duplicate measurements were carried out in the case of DhaA12. In parallel, the estimation of 'time 0' spectrum $\nu(0)$, i.e., the spectrum emitted from the initial Frank-Condon state before any reorientation of the dye microenvironment occurred, was performed. The estimation was based on analysis of the steady-state excitation spectrum recorded in haloalkane dehalogenases and absorption and emission spectra of coumarin 120 recorded in neat solvents. Subtracting the maximum of 'time 0' spectrum $\nu(0)$ and maximum of the spectrum emitted from the relaxed state $\nu(\infty)$, which was gained by the extrapolation of the TRES time dependence $\nu(t)$ to $t \rightarrow \infty$, yielded the dynamic Stokes shift $\Delta\nu$. This parameter proved to be directly correlated with the polarity of the dye microenvironment[18]. When comparing labeled enzymes with, as presented here, identical amino acids in the probe vicinity, the dynamic Stokes shift ($\Delta\nu$) qualitatively reflects the degree of hydration of the solvated protein segments. In addition to $\Delta\nu$, the normalization of the TRES time dependence $\nu(t)$–$\nu(\infty)$ to the overall shift $\Delta\nu$ yields the so-called correlation function, $C(t)$, which is a measure of TDFS kinetics. For the sake of quantification, the integration of $C(t)$ is introduced as integral relaxation time τ_r. This parameter proved to be correlated with the viscosity of the dye microenvironment[18]. In our particular case, the τ_r is inversely related to

© 2014 Nature America, Inc. All rights reserved.

doi:10.1038/nchembio.1502

the mobility of the protein segments in the immediate vicinity of the dye[19]. The majority of the TDFS in the enzymes investigated herein occurs on timescales longer than tens of picoseconds, being substantially slower than the TDFS kinetics reported in pure water[18]. Molecular dynamics simulations indicate that this slow component of TDFS reflects conformational fluctuations of the protein segments that contain charged or partially charged hydrated residues[23,28]. Exchange of individual water molecules in the investigated protein region is invisible for the long-scale TDFS, as demonstrated in detail elsewhere[19].

Crystallographic analysis. *Protein crystallization and data collection*. DhaA12 was crystallized at 4 °C using the sitting-drop vapor-diffusion technique[29]. The sitting drop was prepared by mixing 0.2 mM enzyme in 50 mM Tris-HCl buffer (pH 7.5) and the reservoir solution in a 1:1 ratio. The reservoir solution consisted of 20% (w/v) PEG 4000 and 100 mM MES sodium salt (pH 6.1). Diffraction data were collected at 100 K by a MAR Mosaic CCD camera (Marresearch) from a single crystal on beamline 14.1 at the BESSY-II synchrotron with a wavelength of 0.918 Å. The crystal was mounted directly into nylon loop[30] and flash-frozen in a cold nitrogen stream without additional cryoprotection.

Structure refinement. The structure was solved by the molecular replacement techniques in Molrep[31] using the crystal structure of the mutant haloalkane dehalogenase DhaA04 (PDB code 3FBW) as the template. Crystallographic refinements were carried out using the programs REFMAC5 (ref. 32) and SHELXL[33]. Coot software[34] was used for the manually built part. The isotropic ADP refinement was applied to all of the components (i.e., the enzyme, waters and the chloride ion) and resulted in lower R and R_{free} characteristics. The data collection and refinement statistics are presented in **Supplementary Table 3**.

Molecular modeling. Description of molecular modeling protocols is available in the **Supplementary Note**.

26. Sambrook, J. & Russell, D.W. *Molecular Cloning: a Laboratory Manual.* (Cold Spring Harbor Laboratory Press, New York, 2001).
27. Iwasaki, I., Utsumi, S. & Ozawa, T. *Bull. Chem. Soc. Jpn.* **25**, 226 (1952).
28. Furse, K.E. & Corcelli, S.A. *J. Phys. Chem. Lett.* **1**, 1813–1820 (2010).
29. Ducruix, A. & Giegé, R. *Crystallization of Nucleic Acids and Proteins: a Practical Approach.* (Oxford University Press, New York, 1999).
30. Teng, T.Y. *J. Appl. Crystallogr.* **23**, 387–391 (1990).
31. Vagin, A. & Teplyakov, A. *J. Appl. Crystallogr.* **30**, 1022–1025 (1997).
32. Murshudov, G.N., Vagin, A.A. & Dodson, E.J. *Acta Crystallogr. D Biol. Crystallogr.* **53**, 240–255 (1997).
33. Sheldrick, G.M. *Acta Crystallogr. A* **64**, 112–122 (2008).
34. Emsley, P., Lohkamp, B., Scott, W.G. & Cowtan, K. *Acta Crystallogr. D Biol. Crystallogr.* **66**, 486–501 (2010).

© 2014 Nature America, Inc. All rights reserved.